Study of microstructure and mechanical properties of high performance Ni-base superalloy GTD-111

Seyed Abdolkarim Sajjadi [a],*, Said Nategh [a], Roderick I.L. Guthrie [b]

[a] *Faculty of Materials Science and Engineering, Sharif University of Technology, Azadi Ave., P.O. Box: 11365, Tehran 8639, Iran*
[b] *Department of Mining and Metallurgical Engineering, McGill University, Montreal, Quebec, Canada H3A2B2*

Abstract

The Ni-base superalloy GTD-111 is widely used in manufacturing of the first stage blades of high power land-based gas turbines. In spite of its important role in increasing the performance of gas turbines, due to high temperature capability, there are little data on the microstructure, deformation mechanisms and mechanical properties of the alloy. The aim of present paper is to determine in details these properties. Microstructural characteristics of the alloy were assessed by means of optical, scanning and transmission electron microscopy. The tensile behaviour of GTD-111 has been studied in the temperature range 25–900 °C. The results showed abnormal variations in tensile properties with increasing temperature. TEM observations confirmed that these behaviours were affected by the γ′ properties and a change in the mechanism of deformation of GTD-111 at high temperatures. From creep test results, Larson–Miller and Monkman–Grant plots were produced which are used for life prediction. It was also observed that several creep deformation mechanisms operate at various combinations of temperature and stress. © 2002 Published by Elsevier Science B.V.

1. Introduction

The Ni-base superalloy GTD-111 was designed in the 1970s and employed in the 1980s in high power industrial gas turbines as the first stage blades. Because of its excellent high temperature properties, the alloy was substituted for the previous material, IN738LC, in high power gas turbines operating at higher temperatures. The alloy contains refractory elements such as Mo, W, Ta, Cr and Co to prevent local hot corrosion. It is claimed that the creep strength of GTD-111 is about 20 °C higher than that of IN738LC [1]. Gaudenzi et al. [2] studied oxidation and hot corrosion resistance of both alloys and showed that the corrosion resistance of GTD-111 is the same as that of IN738LC. Also, Daleo et al. [3] reported some technical data for GTD-111.

The alloy is a modification of René 80 and IN738LC. Because of the similarity in composition, microstructure and application between GTD-111 and IN738LC, their properties are compared in this paper. Generally, there are few papers on the Ni-base GTD-111 and for a complete description of the material properties and evaluation of its stability in service condition, more data on the alloy are required. The aim of this investigation is to specify and determine some of the properties of GTD-111. For this reason, some creep-life prediction techniques for these alloys such as Larson–Miller parameter, the Monkman–Grant relationship and its modification are examined. Also, because of extreme conditions during the operation of gas turbine blades, high temperature tensile and creep behaviour are of great interest to investigators and manufacturers and the present study considers them.

2. Experimental procedure

The chemical composition of the Ni-base superalloy GTD-111 was determined by X-ray fluorescence, opti-

* Corresponding author. Fax: +98-21-600-5717.
E-mail address: sajadi@mtl.sharif.ac.ir (S.A. Sajjadi).

cal emission spectroscopy and atomic absorption. All specimens used in the present study were machined out of an investment cast blade made from GTD-111 superalloy subjected to the standard heat treatment. It should be mentioned that the standard heat treatment of this alloy is performed by the manufacturer and there is no any published data on specifications of the heat treatment cycle. More than 30 constant stress creep tests were carried out according to ASTM E139 [4] at temperatures ranging from 760 to 981 °C and stress range of 152–586 MPa. Room and high temperature tensile tests at a constant strain rate of 10^{-4} s^{-1} were performed on 42 specimens according to ASTM E8 and E21 [5,6]. The temperature was measured with two thermocouples placed on the specimen gage length. The temperature variation of the furnaces during creep and tensile tests was about ± 1 °C. Metallographic examination was made on as heat-treated and fractured specimens by means of optical, scanning and transmission electron microscopes. Total γ' weight percent was obtained using the electrolytic extraction technique [7] and the primary γ' volume percent, which is with a good approximation equal to the weight percent, was measured using TEM and SEM micrographs and surface fraction method by image analyzer.

To prepare TEM samples, disks were cut from the gauge length of the specimens deformed at different conditions normal to the loading axis. They were thinned using ion milling machine and electrochemical polishing with a double jet polisher using an electrolyte of 7% perchloric acid and 93% acetic acid at -2 °C. Microstructures were examined in Leitz optical microscope at $1600 \times$, Philips scanning electron microscope at 35 KV and Philips scanning-transmission electron microscope (STEM) at 200 KV.

3. Results and discussion

3.1. Chemical composition

The alloy consists of carbide-forming, γ'-forming and refractory elements. The roles of the alloying elements in Ni-base superalloys have been discussed in several papers [8–12]. The chemical composition of the superalloy GTD-111, in weight percent, is given in Table 1. For the purpose of comparison the chemical composi-

tion of IN738LC is also included. GTD-111 benefits from a good combination of refractory elements and is, therefore, superior in high-temperature properties in comparison with other Ni-base superalloys.

3.2. Microstructure

GTD-111 has a multi-phase microstructure consisting of γ matrix, bimodal γ' precipitates, γ–γ' eutectics, carbides and a small amount of deleterious phases such as: δ, η, σ and Laves. The γ' phase is a superlattice possessing the L1$_2$-type structure with a nominal composition of Ni$_3$(Al,Ti). The primary γ' cuboids with average edge length of 0.8 μm are produced during solidification under 1200 °C. The secondary γ' spheroids of average 0.1 μm diameter are produced during aging after partial solution treatment. The total γ' volume fraction was determined to be more than 60%, using a chemical extraction method. Therefore, the total volume fraction of γ' in GTD-111 is about 15–20% higher than IN738LC. It is worth noting that the total γ' fraction in IN738LC is about 45%.

Carbides are distributed at grain boundaries and uniformly within the grains. Chemical analysis of carbides identifies the carbides formed within grains as mainly MC type carbides, in which M is substituted for Ti, W and Ta. The carbides observed at grain boundaries are M$_{23}$C$_6$ type carbides, in which M is substituted for Cr and Mo. Inside some of the carbides dark spots can be seen. Chemical analysis showed that they are oxides, nitrides or carbonitride particles, which act as nucleation sites for carbides. The serrated grain boundaries prevent grain boundary sliding and enhance creep strength.

The γ–γ' eutectics are distributed at dendrite boundaries, often near micropores, showing that they are formed during the last stages of solidification. The eutectic size varied from 30 to 135 μm and the volume percent was determined to be from 0.15 to 6%, depending on the specimen position in the blade.

The blade used for producing GTD-111 specimen was hipped, however, because of its large size and weight, which was about 13kg. Some micropores with various sizes were observed. These solidification defects, which are common in cast parts, affect mainly ductility scatter.

Table 1
Chemical compositions of GTD-111 and IN738LC superalloys (in wt.%)

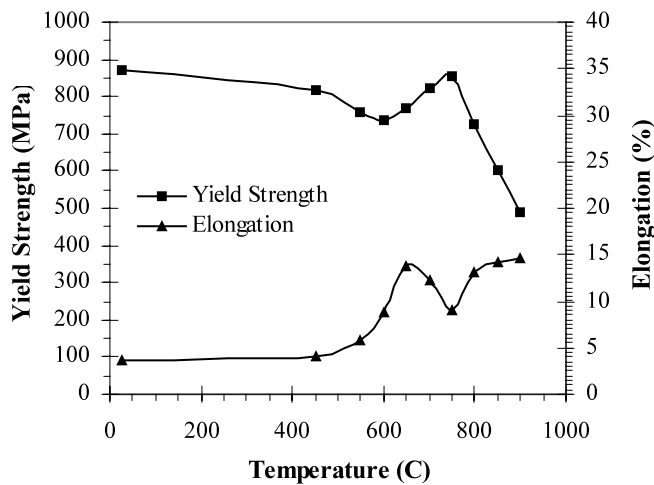|	Ni	Cr	Co	Ti	W	Al	Ta	Mo	Fe	C	B
GTD-111	Bal.	13.5	9.5	4.75	3.8	3.3	2.7	1.53	0.23	0.09	0.01
IN738LC	Bal.	16.0	8.3	3.38	2.6	3.4	1.7	1.70	0.10	0.11	0.01

Fig. 1. Tensile properties of GTD-111 superalloy at different temperatures.
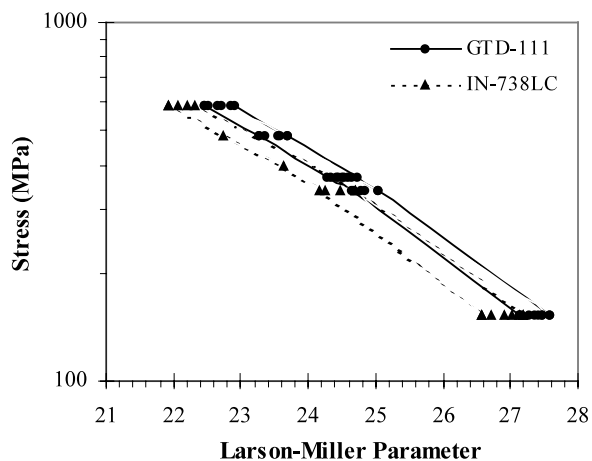

Fig. 2. Larson–Miller parameter diagram for GTD-111 and IN38LC superalloys.

3.3. Mechanical properties

The tensile properties of the alloy in standard heat treatment condition are shown in Fig. 1. Compared with the data reported by Bettge et al. [13] for superalloy IN738LC both alloys show variations in properties with temperature. The variation depends on different deformation mechanisms operating at each temperature [13,14]. The results indicate that the yield strength of GTD-111 exceeds that of IN738LC over the temperature range from 25 to 900 °C. On the contrary, the tensile ductility of GTD-111 is lower than that of IN738LC mainly for two reasons: (1) the volume percent of the refractory elements in GTD-111 is higher; (2) γ' precipitate volume fraction in GTD-111 is about 20% higher.

The creep curves of GTD-111, similar to that of most Ni-base superalloys, show three distinctive regions at temperatures ranging from 760 to 981 °C. The speci-

mens spend a large portion of their lives in the tertiary stage. Using the data obtained from stress-rupture tests constructed at different conditions, several diagrams can be obtained. They are used for creep life prediction of the material operating at high temperatures in which creep is the dominant mode of deformation. The Larson–Miller plot is one method which is accepted as a reliable technique for life prediction so long as the alloy microstructure is stable during prolonged exposure at high temperature [15–18]. Fig. 2 shows the Larson–Miller plot of GTD-111 as compared with that of IN738LC reported by Castillo et al. [15]. In construction of such plot the Larson–Miller parameter P was described as:

$$P = T \times 10^{-3} \, (C + \log t_{\mathrm{r}})$$

where T is temperature in Kelvin or Rankine and C is a constant assumed to be 20. The figure clearly indicates that the stress rupture strength of GTD-111 exceeds that of IN738LC.

The study of GTD-111 microstructure in creep-deformed specimens under high temperature and stress for various times using TEM and SEM showed that the microstructure is stable. Also, to confirm the microstructural stability of the superalloy, a plot showing relationship between time to the onset of tertiary creep, t_{t}, and time to rupture, t_{r}, was constructed from the creep results. It has been reported that for materials which are structurally stable during creep, the ratio $(t_{\mathrm{r}}/t_{\mathrm{t}})$ is about 1.5 and for materials which show structural instability, such as over aging and γ' particle coarsening, during creep the value is higher [19–22]. The ratio for GTD-111 is determined to be 1.76 whereas in the case of IN738LC a ratio of 2.2 has been observed [23]. Comparison of these results confirms that GTD-111 structure is more stable than that of IN738LC.

Thus the Larson–Miller technique should be suitable, with good approximation, for predicting the creep life of GTD-111 by extrapolating the data obtained from high stress–high temperature stress-rupture tests.

Monkman and Grant [24] proposed a relationship between steady state creep rate $(\dot{\varepsilon}_{\mathrm{s}})$ and rupture life (t_{r}) to analyse data obtained from high temperature–high stress uniaxial stress-rupture tests as follows:

$$t_{\mathrm{r}}\dot{\varepsilon}_{\mathrm{s}}^{m} = C$$

where m and C are material constants. If for a given material the constants are determined, the rupture time can be predicted just by measuring the steady state creep rate. This relationship is graphically represented in Fig. 3 for GTD-111. For the purpose of comparison, on this figure the data for IN738LC from another source [16] are superimposed. In this prediction technique the fracture mode, creep deformation mechanism and the failure strain are not considered. Koul et al.
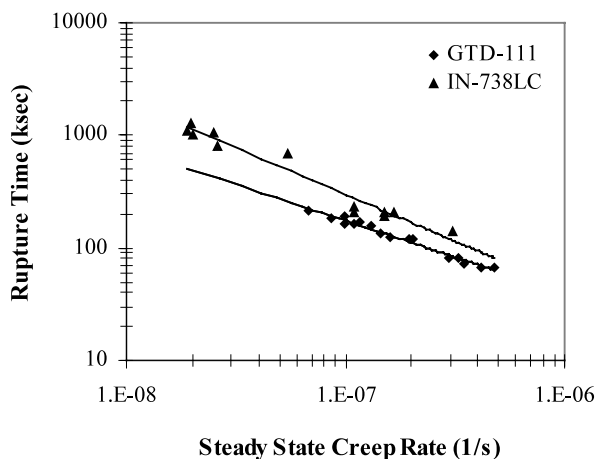
Fig. 3. Steady-state creep rate as a function of rupture time of GTD-111 and IN738LC.
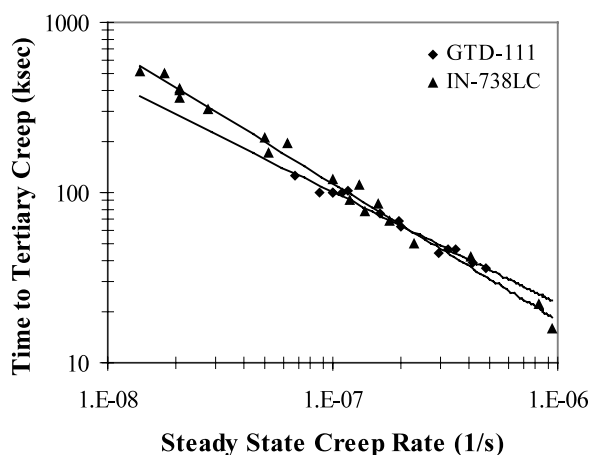

Fig. 4. Time to tertiary creep versus minimum creep rate in GTD-111 and IN738LC.
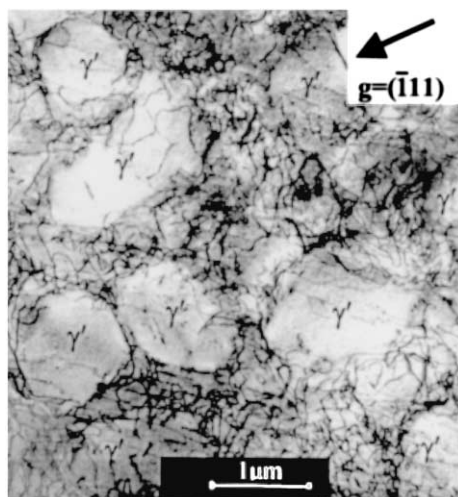

Fig. 5. TEM microstructure of GTD-111, creep-deformed in steady state region in 982 °C/152 MPa, showing dislocation climb mechanism.

[16] in an investigation on creep life predictions in IN738LC (new and serviced materials) claimed that the Monkman–Grant relationship is unable to distinguish degenerative effects caused during service because, in the case of complex alloys, stress rupture data exhibit a wide scatter band. For this reason they proposed a modification for the equation which isolates the tertiary stage creep life and creep strain from creep data. The modified Monkman–Grant equation is written as:

$$t_t = k\dot{\varepsilon}_s^m$$

in which t_t is time to the tertiary creep and m and k are material constants. Fig. 4 shows t_t, the sum of primary and secondary creep lives $(t_p + t_s)$, as a function of the steady state creep rate, $\dot{\varepsilon}_s$, in log–log scale for GTD-111. Also, for comparison with IN738LC the data reported by Castillo et al. [15] are superimposed on the plot.

3.4. Deformation mechanisms

The superalloy GTD-111 is strengthened by two main strengthening mechanisms: solid solution hardening and precipitation hardening. Elements such as: W, Mo, Ta, Ti and Cr are the most potent solid solution strengtheners. Ni, Ti and Al, are γ' formers and together with significant amounts of Mo and W strengthen the alloy through a precipitation hardening mechanism. Some factors such as: coherency strains at $\gamma-\gamma'$ interface, elastic moduli difference between γ' and γ matrix, lattice mismatch, long range ordering of γ' and anti-phase boundary (APB), produced during the movement of dislocations through γ' particles, strengthen the Ni base superalloys via the precipitation hardening mechanism [12,25,26].

In the standard heat treatment condition the microstructure exhibits a low dislocation density at $\gamma-\gamma'$ interfaces. After creep deformation at 982 °C/152 MPa the $\gamma-\gamma'$ interface contains dense concentrations of dislocations with few, if any, dislocations inside the particles. The γ' particles are also tending to become rounded. However, there is no evidence for cutting or deformation of the γ' particles. The dislocation configurations in the grains, which are the representatives of dislocation climb processes, are illustrated in Fig. 5 for GTD-111 specimens creep-tested at medium stresses. It is clearly shown that dislocations migrate mainly within the γ matrix in creep processes and many dislocation networks, after climbing over γ' particles, exist at $\gamma-\gamma'$ interfaces. There is no evidence that dislocations cut through γ' particles. This figure also shows a homogeneous distribution of low-density dislocations within the matrix phase, network formation at the $\gamma-\gamma'$ interfaces with little or no dislocations in the γ' particles.

Therefore, at medium stresses the dislocations are unable to cut through or bow between the particles.
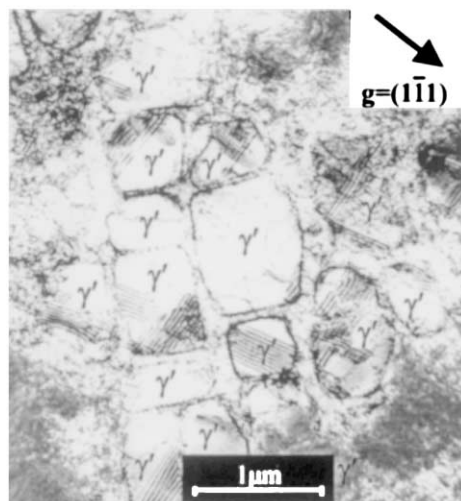
Fig. 6. TEM microstructure of GTD-111, creep-deformed in steady state region in 760 °C/586 MPa, showing stacking fault formation.

Deformation is based now on the movement of dislocations in the matrix and the change of the γ' morphology [27]. In this region the dislocations are forced to overcome the particles by climb.

The results of studies on creep-tested specimens interrupted during steady-state-creep using TEM show that at high stresses dislocations cut through γ' particles by stacking fault (SF) formation and APB coupled dislocation pairs, depending upon the amount of creep strain. The creep-induced dense dislocation networks are mainly constrained at the γ–γ' interface. Fig. 6 shows the TEM microstructure of the specimen creep-tested in the shear dislocation creep region at 760 °C/586 MPa. As can be seen, stacking faults are formed inside γ' particles, demonstrating the shear dislocation creep mechanism operating in this condition. In this case, because the creep strain was low, no APB coupled dislocation pairs were observed. Sajjadi and Nategh [28] have studied creep behaviour of the Ni-base superalloy GTD-111 and released some detailed data on different mechanisms operating under different creep conditions. They obtained three different activation energies at high temperatures for grain-boundary diffusion creep, dislocation climb, and shear mechanisms.

4. Conclusions

The aim of this investigation was to study of microstructure and mechanical properties of the Ni-base GTD-111. In this regard many tensile and creep-rupture tests at different temperatures were carried out on specimens prepared from a turbine blade. The tensile test results showed that there are fluctuations in strength and ductility with respect to temperature. TEM investigation on the fractured tensile specimens

indicated that the deformation mechanisms operating at each region are the main factors for the behaviour. The microstructural observations of creep-deformed specimens identified different mechanisms of interaction between dislocations and γ' precipitates in GTD-111. The occurrence of a given mechanism depends on the test conditions of temperature and stress. A shear mechanism involving stacking fault and anti-phase boundary coupled dislocation pair formation in the γ' precipitates occurs at high stresses. Dislocation climb over γ' precipitates and diffusional creep through grain boundaries are the other mechanisms operating at lower stresses.

The mechanical properties study demonstrated the superiority of GTD-111 over IN738LC. In addition, it was indicated that GTD-111 is microstructurally more stable. These properties make GTD-111 more reliable for use at high temperatures.

References

[1] P.W. Schilke, A.D. Foster, J.J. Pepe, A.M. Beltran, Aspects of the drainage of aqueous humor in cats. Adv. Mater. Process. 1992, 4, p. 22.
[2] G.P. Gaudenzi, A. Colombo, G. Rocchini, F. Uberti, Proceedings of the Conference Elevated Temp. Coatings, Sci. and Tech. II, California, USA, 4–8 Feb. 1996, p. 301.
[3] J.A. Daleo, J.R. Wilson, J. Eng. Gas Turbines Power Trans. ASME 120 (1998).
[4] ASTM E139, Standard Test Methods for Conducting Creep, Creep–Rupture, and Stress-Rupture Tests of Metallic Materials, 1998.
[5] ASTM E8, Standard Test Methods for Tension Tests of Metallic Materials [Metric], 1998.
[6] ASTM E21, Standard Test Methods for Elevated Temperature Tension Tests of Metallic Materials, 1998.
[7] R.A. Stevens, P.E.J. Flewith, J. Mater. Sci. 13 (1978) 367.
[8] C.R. Brooks, Heat Treatment, Structure and Properties of Non-Ferrous Alloys, American Society for Metals, Metals Park, OH, 1982, p. 139.
[9] J.L. Smialek, G.M. Meier, in: C.T. Sims, N.S. Stoloff, W.C. Hagel (Eds.), Superalloys II, Wiley, New York, 1987, p. 291.
[10] T.P. Gabb, R.L. Dreshfield, in: C.T. Sims, N.S. Stoloff, W.C. Hagel (Eds.), Superalloys II, Wiley, New York, 1987, p. 575.
[11] W. Betteridge, J. Heslop, The Nimonic Alloys and other Nickel-Base High Temperature Alloys, Edward Arnold, Bristol, UK, 1974, p. 45.
[12] D.P. Pope, S.S. Ezz, Int. Met. Rev. 29 (1984) 136.
[13] D. Bettge, W. Osterle, J. Ziebs, Z. Metallkd 86 (3) (1995) 190.
[14] S.A. Sajjadi, S. Nategh, M. Isac, Can. Metall. Q., May. 2001 (Submitted).

[15] R. Castillo, A.K. Koul, E.H. Toscano, J. Eng. Gas Turbines Power 109 (1987) 99.

[16] A.K. Koul, R. Castillo, K. Willett, Mater. Sci. Eng. 66 (1984) 213.

[17] C.G. Bieber, J.R. Mihalisin, Second International Conference on the Strength of Metals and Alloys, American Society for Metals, Metals Park, OH, 1970, p. 1031.

[18] F.R. Larson, J. Miller, Trans. ASME 74 (1952) 765.

[19] J.P. Dennison, P.D. Holmes, B. Wilshire, Mater. Sci. Eng. A33 (1978) 35.

[20] P.W. Davies, B. Wilshire, Iron & Steel Inst. Special Report, 1960, p. 34.

[21] J.P. Dennison, B. Wilshire, J. Inst. Met. 91 (1962) 343.

[22] K.R. Williams, B. Wilshire, Mater. Sci. Eng. A28 (1977) 289.

[23] G. Jianting, D. Ranucci, E. Picco, P.M. Strocchi, Met. Trans. A 14 (1983) 2329.

[24] F.C. Monkman, N.J. Grant, Proc. ASTM 56 (1956) 593.

[25] P.J. Henderson, M. McLean, Acta Met. 31 (1993) 1203.

[26] R.A. Stevens, P.E.J. Flewitt, Acta Met. 29 (1981) 867.

[27] M. Feller-Kniepmeier, T. Link, Met. Trans. A 20 (1989) 1233.

[28] S.A. Sajjadi, S. Nategh, Mater. Sci. Eng. A307 (2001) 158.